Light scattering by microdroplets of water and water suspensions

Daniel Jakubczyk, Marcin Zientara, Gennadiy Derkachov, Krystyna Kolwas and Maciej Kolwas*
Institute of Physics of the Polish Academy of Sciences, al. Lotników 32/46, 02-668 Warsaw, Poland

ABSTRACT

We investigated elastic light scattering on isolated evaporating droplets of radius between 1 and 20 μm. The droplets were either pure water or a water based suspension, they carried electric charge and were contained in an electrodynamic trap. The evolution of the trapped droplet was investigated by means of scatterometry. A numerical model of such evolution, incorporating the kinetic effects near the droplet surface was constructed. For water droplets with spherical inclusions the radius as well as effective refractive index was determined. An essential deviation, in the form of a resonance, from predictions by standard effective medium theories was encountered. Simple analysis of the phenomenon was conducted and a qualitative explanation is proposed. Similar analysis was applied to fullerene water suspension droplets in order to investigate the real part of refraction index.

Keywords: charged droplet, electrodynamic trap, microparticle levitation, mass accommodation coefficient, thermal accommodation coefficient

1. INTRODUCTION

The observation of light scattered on various objects is a most common method of investigation of the reality. In this paper we study the scattering of light on water and water suspensions particle of the fundamental, ideal shape of a sphere, with the radius comparable to the wavelength of the used light – a few micrometers. Under normal atmospheric conditions - below 100% relative humidity S - the droplets of pure water are not stable. They grow for $S>1$ or shrink for $S<1$. Careful observation of light scattering together with the appropriate use of theory allows to determine the radius and the refraction index n (or dielectric function ε: $\varepsilon=n^2$) of the droplet. The issue of refractive index is especially interesting for droplets of suspensions, which are so omnipresent. In the first part of this paper we present the study of evolution of pure water microdroplet with well known refraction index. This investigation made it possible to look into kinetic regime of droplet evolution - the region of droplet sizes of the order of the free path of air molecules. In this region it is necessary to supplement diffusion coefficient with so called evaporation coefficient α_C describing the ratio of the number of molecules crossing the liquid-vapor interface to the number of molecules impinging on it: $\alpha_C = n_{evap}/n_{col}$. Similarly, the thermal conductivity of moist air must be supplemented with the thermal accommodation coefficient α_T, determines the probability that a molecule on impinging the interface attains the thermal equilibrium with the medium on the opposite side. The literature yields a very imprecise value for α_C and α_T ranging from 0.01 to 1 (compare e.g.: [1, 2, 3, 4]). The aim of our first experiments was to find the value of α_C and α_T.

2. MODEL

The evaporation of droplets has been widely discussed, also taking kinetic effects into account (see e.g.: [3, 4, 5, 6]). The evolution of the droplet is driven by the gradients of temperature and water vapor density near the droplet surface. However, water mass transport up to the distance comparable to the mean free path of air molecules from the droplet surface $a<r<a+\Delta$ ought to be described with gas kinetic expressions (Δ is of the order of the mean free path of air molecules [4]). For $r\geq a+\Delta$ the diffusional transport of the water vapor should be considered.

The droplet mass m change is equal to the flux of water through the droplet surface:

* Send correspondence to Maciej Kolwas; E-mail: kolwas@ifpan.edu.pl

$$\frac{dm}{dt} = -J(r=a) \ . \tag{1}$$

Therefore the equation of evolution of droplet radius can be written as:

$$\frac{da}{dt} \equiv \dot{a} = \frac{D_K}{\rho_L a}\left[\rho_\infty - \rho(r=a)\right], \ D_K = \frac{D}{\frac{a}{a+\Delta} + \frac{D}{a\alpha_C}\sqrt{\frac{2\pi M}{RT_a}}} \tag{2}$$

where ρ_L is liquid water density and $\rho(r=a)$ and ρ_∞ are water vapor densities on the droplet surface and far from that surface respectively. D_K is an effective diffusion coefficient, equal to the diffusion constant D for sufficiently large droplets, T_a is temperature of the droplet, M is the water molecular mass and R is the universal gas constant. Expressing vapor density far from the droplet by means of saturated vapor pressure p_S at a given temperature leads to

$$\rho(r \to \infty) = S\frac{M}{R}\frac{p_S(T_\infty)}{T_\infty} \tag{3}$$

where S is the relative humidity, T_∞ is the temperature far from the droplet. Similarly

$$\rho(r=a) = \frac{M}{R}\frac{p_S(T_a)}{T_a}\exp\left[\frac{M}{RT_a\rho}\left(\frac{2\gamma}{a} - \frac{Q^2}{32\pi^2\varepsilon_0 a^4}\right)\right] \tag{4}$$

is the vapor density near the charged droplet surface, where γ is the surface tension of water, Q is the charge of the droplet and ε_0 is the permittivity of vacuum. Finally time evolution of the droplet radius is:

$$\dot{a} = \frac{MD_K(a,T_a)}{Ra\rho}\left\{S\frac{p_S(T_\infty)}{T_\infty} - \frac{M}{R}\frac{p_S(T_a)}{T_a}\exp\left[\frac{M}{RT_\infty\rho}\left(\frac{2\gamma}{a} - \frac{Q^2}{32\pi^2\varepsilon_0 a^4}\right)\right]\right\} . \tag{5}$$

Similar procedure for the transport of heat leads to the equation describing evolution of temperature:

$$\dot{T}_a = \frac{3}{a^2 c_W}\left[qa\dot{a} - \frac{\lambda_K(a,T_a)}{\rho_L}\left(T_a - T_\infty\right)\right], \ \lambda_K = \frac{\lambda}{\frac{a}{a+\Delta_T} + \frac{\lambda}{a\alpha_T\rho_A c_P}\sqrt{\frac{2\pi M_A}{RT}}} \tag{6}$$

where c_W and q are specific heat capacity and latent heat of evaporation of water respectively, λ, ρ_A, c_P and M_A are thermal conductivity, density, specific heat capacity under constant pressure and molecular mass of moist air respectively and Δ_T is the 'thermal jump' distance.

Thus, the model of evaporation utilized in our analysis consists of two equations describing the transport of water mass (5) and heat (6) between the droplet and its surroundings. Additionally we must remember about Rayleigh's condition [5]– the fissility parameter X ought to be smaller than 1:

$$X = \frac{E_Q}{2E_\gamma} = \frac{Q^2}{64\pi^2 \varepsilon_o \gamma \cdot a^3} < 1 \tag{7}$$

where E_Q and E_γ are the Coulomb and surface tension energies respectively.

It is worth noting that without the Rayleigh's condition the equation set (5)-(6) predicts the asymptotic stabilization of evaporating droplet radius $\dot{a} \to 0$ for $a \to a_{end}$, given by the equation:

$$\ln S = \frac{M}{\rho R T_\infty}\left(\frac{2\gamma}{a_{end}} - \frac{Q^2}{32\pi^2 \varepsilon_0 a_{end}^{\ 4}}\right). \tag{8}$$

3. EXPERIMENT

The experimental setup is presented in figure 1. A detailed description can be found in our previous papers [7]. Paul trap kept in the climatic microchamber is the heart of the system. Water droplets are injected into the trap. The light scattered by the trapped particle was collected through the port in the ring electrode with the microscope objective positioned in the scattering plane at right angle from the direction of the incident beams (see figure 2). The numerical aperture of the system was ~0.17. The first experiments were conducted with pure water (20 ppb total dissolved substances) at temperatures of 13.7 °C and 13.1 °C, atmospheric pressure of 1006 hPa and the charge Q of the order of 5×10^5 elementary charges. We registered the scaterograms of the evaporating droplet. Then with the aid of the Mie theory the time dependence of droplet radius was determined (see figures 3 and 4).

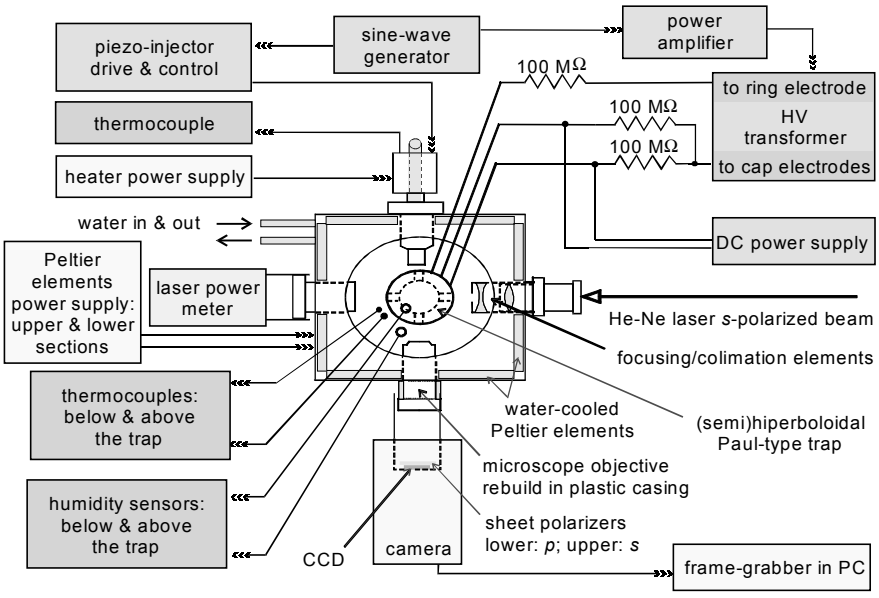

Figure 1. Experimental setup diagram.

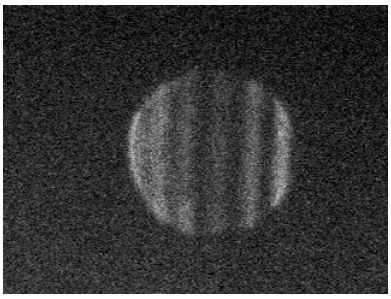

Figure 2. An example of observed scattered light. The fitting of the interference fringes pattern with the Mie theory enables simultaneous determination of the radius and the refractive index of the droplet.

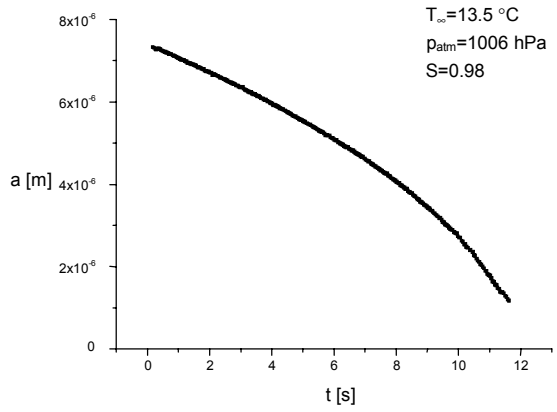

Figure 3. Evaporation of pure water droplet.

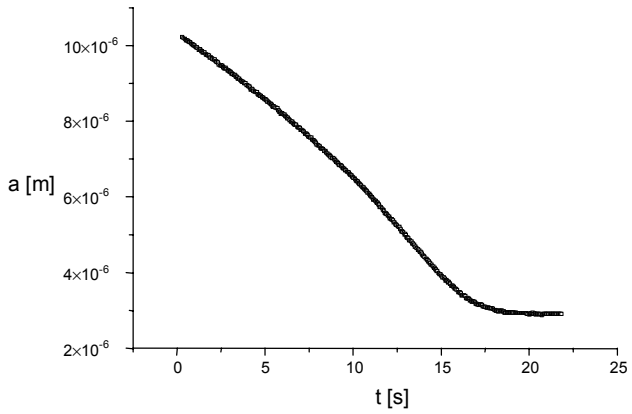

Figure 4. Evaporation of a contaminated water droplet. The stabilization of the radius for S<1 is possible due to the reduction of the vapor pressure over the curved surface caused by the dissolved or surface active substances.

From the time dependence of the radius $a(t)$ we can determine the value of the mass accommodation coefficient α_C =0.12±0.01, the thermal accommodation coefficient α_T = 0.65±0.09 as well as the very precise value of the relative humidity.

4. LOCAL-FIELD RESONANCE IN LIGHT SCATTERING BY A SINGLE WATER DROPLET WITH SPHERICAL DIELECTRIC INCLUSIONS

In the second type of experiment we used the following suspensions of nanospheres in water: (i) porous silica (refractive index n=1.45) of 300 and 450 nm diameter and (ii) polystyrene (n=1.58) of 200 nm diameter. Vertically polarized 632.8 nm He-Ne laser light was scattered on a single levitated droplet of suspension. We registered the light scattering patterns on *s* and *p* polarizations (perpendicular and parallel to the scattering plane respectively) simultaneously. The signal in *p* polarization appears when the levitated particle depolarizes light. Since water was evaporating from the droplet, we could observe the transition from scattering on a diluted suspension through scattering on a concentrated suspension to scattering on a dry nanospheres agglomerate or a finite-size highly imperfect photonic crystal. In the first case we observed a Mie scattering pattern appearing on *s* polarization only (see figure 5a); the second (figure 5b) is characterized by a speckled Mie scattering pattern and in the third (figure 5c) we can see bulk speckle or imperfect Kossel lines [8] that are totally depolarized.

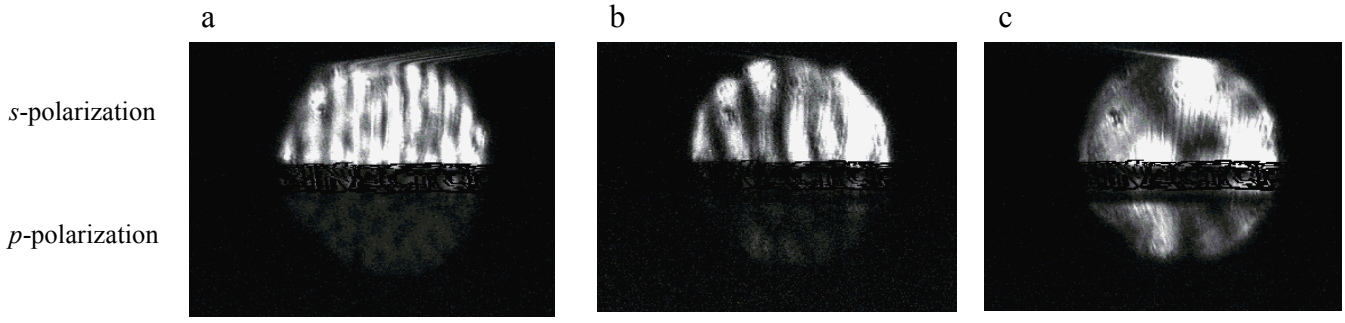

Figure 5. Examples of the scattering patterns observed during evaporation of water from the droplet for low, medium and high concentration of inclusions respectively.

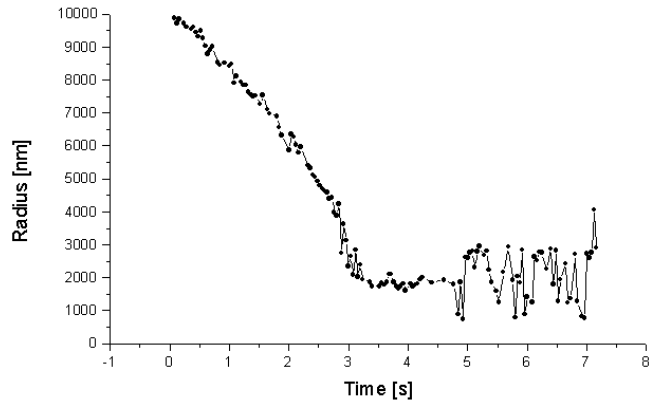

Figure 6. Evolution of the droplet with spherical inclusions. The radius of the droplet was determined with FFT from the scattering pattern. Three regions: normal evaporation, stabilization of the radius and the dry "crystal" can be clearly seen.

The spatial frequency of interference fringes for *s* light polarization is nearly insensitive to the refractive index of the droplet while it exhibits nearly linear dependence on its radius. It is then convenient to determine the radius of the droplet with the aid of FFT [9]. In this way we obtain the evolution of the droplet radius $R(t)$ (see figure 6). In the following part of this paper we use R instead of a for effective radius of the particle, reserving a for inclusion radius. On the other hand, the (averaged) intensity of the scattered light I_{tot} depends on the effective index of refraction of the droplet m_{eff}. We assume that for initial R the concentration of inclusions in suspension is so small that we can put $m_{\mathrm{eff}} = m_{\mathrm{w}}$ (refractive index of water). This enables us to fix the scaling factor of the fit. We ascribe all the variation of I_{tot} to the changes in the real part of m_{eff} and we find m_{eff} by fitting I_{tot} with appropriately averaged Mie scattering formulas. In figure 7 we present the results obtained for three experimental cases, for three values of the radius of inclusion spheres and two types of inclusion material.

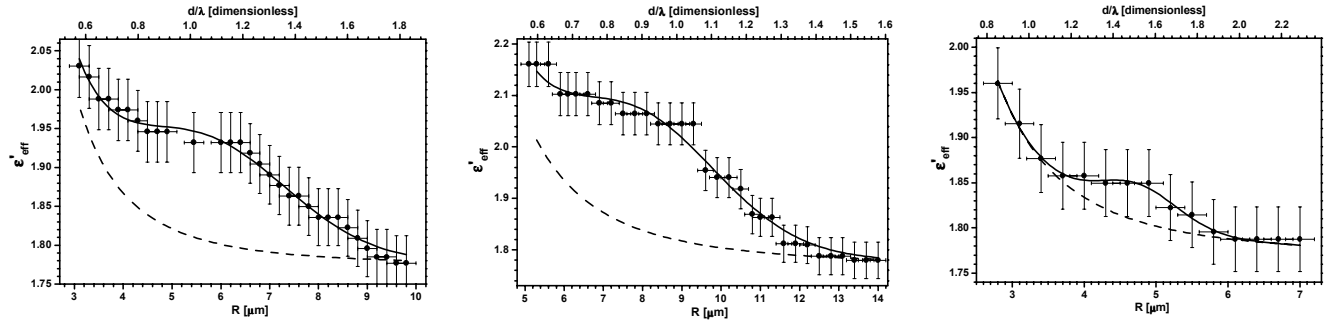

Figure 7. The real part of the effective dielectric function $\varepsilon_{\mathrm{eff}}$ as a function of the droplet radius R for polystyrene inclusions of a=200 nm, and silica inclusions of a=300 nm and a=450 nm.

In order to further interpret the results we use the Lorentz effective field theory, following Kreibig [10], but modifying the model slightly and introducing the local field correction $M(R)$. The effective electric field of light at the position of a given inclusion can be expressed as a Lorentz local field:

$$E_{local} = E_{Mie} + \Delta E \ , \tag{10}$$

where E_{Mie} is the light electric field inside the spherical water droplet (medium) and ΔE is the field created by polarization charges on the Lorentz sphere:

$$\Delta E = \frac{P}{3\varepsilon_0 \varepsilon_m} \ , \tag{11}$$

ε_m is the dielectric function of the medium (water). Polarization P of monodisperse spherical inclusions is

$$P = n \cdot \alpha \cdot M(R) \cdot E_{local} \ , \tag{12}$$

where n is the number density of inclusions and α is the inclusion particle polarizability. The factor $M(R)$ accounts for modification of the local field arising from several phenomena like near field effects, multipolar scattering on inclusion and an effect which seems to be very important – interference of fields scattered on different inclusions. Modification of polarization P leads to the modified Lorentz-Lorenz formula:

$$\varepsilon_{eff} = \varepsilon_m \cdot \frac{1 + \dfrac{2 \cdot n \cdot \alpha \cdot M(R)}{3 \cdot \varepsilon_0 \varepsilon_m}}{1 - \dfrac{n \cdot \alpha \cdot M(R)}{3 \cdot \varepsilon_0 \varepsilon_m}} \ . \tag{13}$$

Introducing a filling factor $f(R) = \dfrac{3V_{incl}}{4\pi R^3}$ (V_{inc} is the total volume of inclusions) enables to express the Lorentz-Lorenz formula in the form proposed by Wiener:

$$\frac{n\alpha}{3 \cdot \varepsilon_0 \varepsilon_m} = f(R) \frac{\varepsilon - \varepsilon_m}{\varepsilon + 2\varepsilon_2} \ , \tag{14}$$

where ε is the dielectric function of inclusion. By combining equations (12) and (14), we obtain the modified Lorentz-Lorenz formula in the form convenient for the present application:

$$\varepsilon_{eff} = \varepsilon_m \cdot \frac{1 + 2 f(R) M(R) \dfrac{\varepsilon - \varepsilon_m}{\varepsilon + 2\varepsilon_2}}{1 - f(R) M(R) \dfrac{\varepsilon - \varepsilon_m}{\varepsilon + 2\varepsilon_2}} \ . \tag{15}$$

The simplest case of M=1 is presented in figure 7 - dashed line. In comparison to this, the experimentally obtained results exhibit a hump that could not be imitated for M=1. This most probably implies that the local light field encounters resonant conditions. Such resonant behavior is possibly not a near-field effect or an effect of the compound droplet surface, because we would expect their influence to grow with diminishing droplet radius. For very small f (small amount of inclusions in water) as well as for f approaching unity (nearly dry crystal composed of former inclusions) M should approach unity. For the sake of a simple analysis we apply a Gaussian curve type correction for M:

$$M(R) = 1 + P_1 \exp\left\{ -2\left[(R - P_2) / P_3 \right]^2 \right\}, \tag{16}$$

where $P_1...P_3$ are optimization parameters. Than we fit $M(R)$ to the experimental data (solid curves in figure 7). The upper abscissas are scaled in a dimensionless average distance between neighboring inclusions d/λ where geometrical distance d between neighboring inclusions is given by $d \approx 2(R^3/N)^{1/3}$ and λ is the wavelength of light in the water medium. It is worth noting that the maximum appears, as could be expected, when the distance between neighboring inclusions is of the order of the wavelength of light in the medium. The variations of position of resonance seem to originate from differences in inclusion sizes and refractive indices. The effect can be understood qualitatively if we consider a resonator consisting of two thick dielectric plates separated by a dielectric medium: for thicker plates (such as for 450 nm diameter inclusions) a resonance associated with reflection from outer surfaces of the plates may manifest separately.

4. LIGHT SCATTERING ANALYSIS OF WATER FULLERENE SUSPENSION

In the experiment of the third type we studied light scattering at two wavelengths: red and green, on a droplet of water fullerene (C_{60}) suspension. We determined the evolution of the droplet radius first. Two examples of such evolution are shown figure 8.

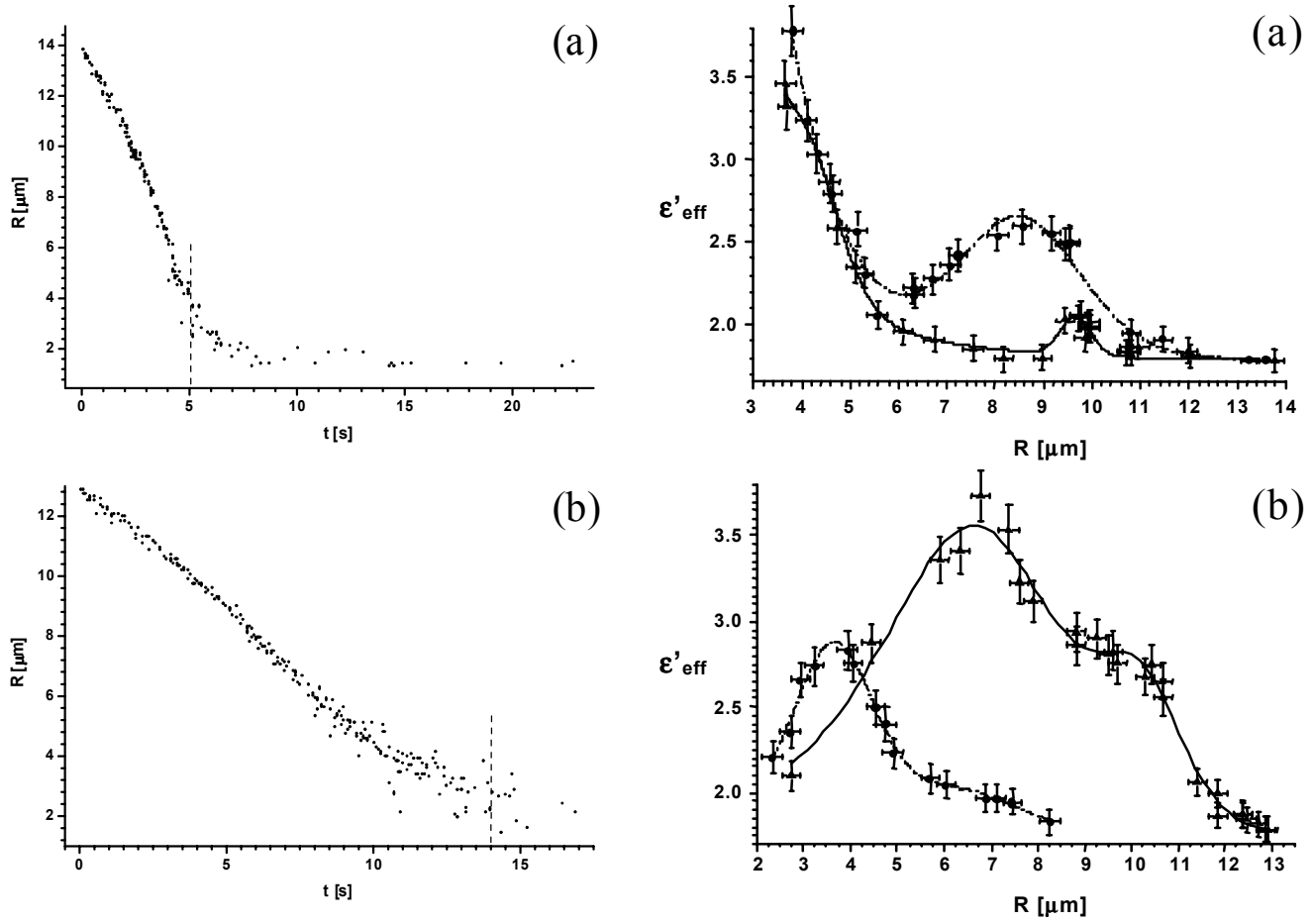

Figure 8. Left: the evolution of the radius of C_{60} water suspension droplet, for high (a) and low (b) initial fullerene contents. The vertical dashed lines show approximately the boundary of wet particle region. Right: the real part of the effective dielectric function of the composite droplet as a function of droplet radius; circles and dash-dot line, green light scattering; triangles and solid line, red light.

The experimental data – effective dielectric function as a function of radius - has been fitted with formulas (15) and (16) where $M(R)$ accounted for two gaussian resonaces this time. The comparison of red and green scattering allowed us to attribute these resonances to (diminishing) average distance between neighboring scatterers (fullerene nanocrystallites). We also tried to infer about the size of scatterers involved. For that we needed V_{incl} which was known only for the case presented in figure 8a, where the particle got completely dry. We assumed the aggregation to be diffusion limited, though the aggregation scenario, is not fully known. Elementary reasoning yields the radius of inclusion to be ~34 nm in that case.

5. CONCLUSIONS

The elastic scattering of coherent light is a powerful tool for the investigation of properties and structure of microdroplets. Careful analysis of the scattered light enables to find the radius and refractive index of the droplet and follow the evolution and evolution dynamics of these quantities. Analysing the dynamics of the radius evolution and applying a suitable thermodynamic model enables finding such parameters of the evolution like mass and heat accommodation coefficients, pertaining to kinetic effects manifesting for very small droplets. On the other hand studying the evolution of effective refractive index, and utilizing a simple model, enables inferring about the internal structure of the droplet of suspension as well as this structure evolution.

ACKNOWLEDGMENT

This work has been supported by Polish State Committee for Scientific Research grant 3 P04G 052 22.

REFERENCES

1. Y. Q. Li, P. Davidovits, Q. Shi, J.T. Jayne, C. E. Kolb and D. R. Worsnop, "Mass and thermal accommodation coefficients of H_2O (g) on liquid water as function of temperature," *J. Phys. Chem. A* **105**, pp. 10627-10634, 2001.
2. R. Shaw and D. Lamb, "Experimental determination of the thermal accommodation and condensation coefficients of water," *J. Chem. Phys.* **111**, pp. 10659-10663, 1999.
3. Y.-S. Zou and N. Fukuta, "The effect of diffusion kinetics on the supersaturation in clouds," *Atmos. Res.* **52**, pp. 115-141, 1999.
4. H. R. Pruppacher and J. D. Klett, *Microphysics of Clouds and Precipitation*, Kluwer, Dordrecht, 1998.
5. N. A. Fuchs, *Evaporation and Droplet Growth in Gaseous Media*, Pergamon, London, 1959.
6. A.V. Kozyrev and A.G. Sitnikov, "Evaporation of a spherical drop in a middle pressure gas," *Uspekhi Fizicheskikh Nauk* **171**, pp. 765-774, 2001.
7. D. Jakubczyk, M. Zientara, W. Bazhan, M. Kolwas and K. Kolwas, "A device for light scatterometry on single levitated droplets," *Opto-Electron. Rev*. **9**, pp. 423-430, 2001.
8. T. Yoshiyama and I. Sogami, "Kossel images as direct manifestation of the gap structure of the dispersion surface for colloidal crystals," *Phys. Rev. Lett.* **56**, pp. 1609-1612, 1986.
9. B. Steiner, B. Berge, R. Gausmann, J. Rohmann and E. R Rühl, "Fast in situ sizing technique for single levitated liquid aerosols," *Appl. Opt.* **38**, pp. 1523—1529, 1999.
10. U. Kreibig and M. Vollmer *Optical properties of metal clusters*, Springer, Berlin, 1995.